Proceedings of the 2007 IEEE
International Conference on Robotics and Biomimetics
December 15 -18, 2007, Sanya, China

Haptic Simulation of Flexible Needle Insertion*

Xuejian He, Yonghua Chen and Libo Tang
Department of Mechanical Engineering
The University of Hong Kong
Pokfulam Road, Hong Kong, China
yhchen@hku.hk

***Abstract* - A flexible needle insertion simulation with force feedback is proposed. The objectives of this simulation are to evaluate the influence of needle parameters (length, radius) to insertion process and train users to better understand the process. Needle buckling will be witnessed while inserting a slender needle into tissue if the exerted force is larger than the critical force of a given flexible needle. Needle buckling can greatly affect the insertion performance, and it can also be utilized to control the insertion path inside tissue. This simulation system can assist users to choose appropriate needle parameters, and train them to be familiar with the process of flexible needle insertion, which is different from traditional needle insertion. Efficient modeling methods for tissue deformation, needle buckling and deflection, haptic rendering are proposed. An experimental simulator based on the proposed methods is developed.**

Keywords: flexible needle, haptics, needle insertion, buckling

I. INTRODUCTION

Percutaneous insertion of needles is one of the most common procedures encountered in clinical practice. Such procedures usually involve inserting slender needles into soft and inhomogeneous tissue with limited visual feedback. Medical students typically learn such procedures by performing them on real patients. Computer simulation systems as an alternative means for medical training have increasingly attracted researchers' attention. However, it is still an open research topic to faithfully simulating the procedure since it involves tissue deformation, needle-tissue interaction, needle deflection and tool force modeling. It requires much knowledge on mechanics, medicine, biology, and computer. Though much work has been done, e.g. [5~8], the simulation of flexible needle buckling and deflection during needle insertion is less studied. Needle buckling is commonly observed and can greatly affect the insertion performance, and it can also be utilized to control the insertion path in tissue. Sometimes, the buckling should be avoided because unexpected force change will make the needle deviate the anticipated path. Such sudden movement might result in damage with surround vital tissue, such as nerve and artery. Therefore, in this paper a flexible needle insertion simulator is proposed as depicted in Fig. 1, in which a user can feel the process of needle buckling and deflection. When buckling occurs, the needle deflects and the feedback force sent to a user through a haptic stylus fluctuates suddenly. The virtual environment of the simulation is mainly composed of three parts: tissue modeling, needle modeling, and haptic rendering, which are explained in the following sections.

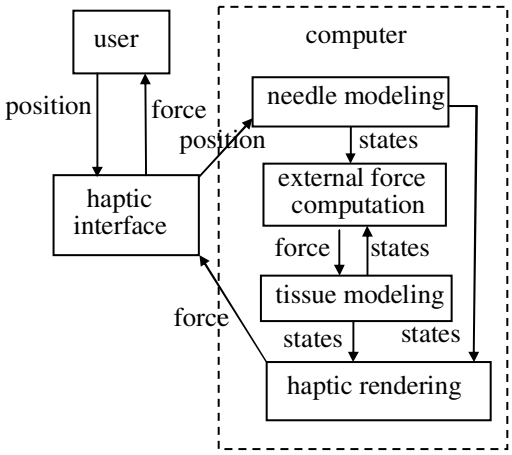

Fig. 1. Block diagram of flexible needle insertion simulation.

II. SOFT TISSUE MODELING

Because linear elasticity models are computationally cheap and physically realistic, they are commonly used in simulation of soft tissue deformation. However, linear models are not suitable for large deformations, because it results in "ghost force", making elements artificially inflate. To solve this problem a co-rotational FEM is proposed by Müller [1] by multiplying the stiffness matrix with element rotations of a local frame with respect to its initial orientation. The following sections explain a modified method used in our simulation.

A. Co-rotational FEM

Within each tetrahedral element e, the displacement field is linearly interpolated as

$$\boldsymbol{u}(\boldsymbol{x}) = \boldsymbol{H}_e(\boldsymbol{x}) \cdot \boldsymbol{u}_v \quad (1)$$

where $\boldsymbol{H}_e(\boldsymbol{x})$ is a 3×12 matrix that contains the shape functions of the tetrahedral element and $\boldsymbol{u}_v$ is the collection of the displacement vectors at the four vertices of the tetrahedron.

* This work is supported by a grant from Hong Kong Research Grants Council under the code HKU 71090E.

Using Cauchy's linear strain tensor [3], for the strain within the tetrahedron we get:

$$\boldsymbol{\varepsilon} = \boldsymbol{B}_e \cdot \boldsymbol{u}_v \tag{2}$$

where $\boldsymbol{B}_e$ is a constant 6×12 matrix. Using Hooke's law, for the stress within an element we get

$$\boldsymbol{\sigma} = \boldsymbol{E} \cdot \boldsymbol{\varepsilon} = \boldsymbol{E}\boldsymbol{B}_e\boldsymbol{u}_v \tag{3}$$

where $\boldsymbol{E}$ is a 6×6 matrix which-for isotropic materials-only depends on two scalars, Young's modulus and Poisson's ratio. Using Cauchy strain, the forces $\boldsymbol{f}_e$ acting on the nodes of an element are derived from the strain energy:

$$\boldsymbol{f}_e = \boldsymbol{K}_e\boldsymbol{u}_v = V_e\boldsymbol{B}_e^T\boldsymbol{E}\boldsymbol{B}_e\boldsymbol{u}_v \tag{4}$$

where the 12×12 matrix $\boldsymbol{K}_e$ is the stiffness matrix and $\boldsymbol{V}_e$ the volume of the element. As mentioned at the beginning of this section, this linear nodal force will make tissue inflate when largely deformed. A warped stiffness approach is proposed by [1]. Let us assume that we know the rotational part $\boldsymbol{R}_e$ of the deformation of the tetrahedron. Then the nodal force is rewritten as:

$$\boldsymbol{f}_e^{'} = \boldsymbol{R}_e\boldsymbol{K}_e(\boldsymbol{R}_e^{-1}\boldsymbol{x} - \boldsymbol{x}_0) = \boldsymbol{R}_e\boldsymbol{K}_e\boldsymbol{R}_e^{-1}\boldsymbol{x} - \boldsymbol{R}_e\boldsymbol{K}_e\boldsymbol{x}_0 = \boldsymbol{K}_e^{'}\boldsymbol{x} + \boldsymbol{f}_{e0} \tag{5}$$

where $\boldsymbol{R}_e$ is a 12×12 matrix that contains four copies of the 3×3 rotation matrix along its diagonal, $\boldsymbol{K}_e^{'}$ is the element's rotated stiffness matrices, and $\boldsymbol{f}_{e0}$ is the force offsets. Finally, the $3n$×$3n$ dimensional stiffness matrix $\boldsymbol{K}$ of the entire mesh is an assembly of the individual $\boldsymbol{K}_e^{'}$ of all the elements.

$$\boldsymbol{K} = \sum_e \boldsymbol{K}_e^{'} \tag{6}$$

Using the linearized elastic forces, the linear algebraic equation of motion for an entire mesh becomes:

$$\boldsymbol{M}\ddot{\boldsymbol{u}} + \boldsymbol{D}\dot{\boldsymbol{u}} + \boldsymbol{K}\boldsymbol{u} = \boldsymbol{f}_{ext} \tag{7}$$

where $\boldsymbol{M}$ is the $3n$×$3n$ dimensional mass matrix, $\boldsymbol{D}$ is the $3n$×$3n$ dimensional damping matrix, and $\boldsymbol{f}_{ext}$ is a vector of external forces. Then, a conjugate gradient algorithm is used to iteratively solve the sparse linear equation system.

B. *External force $\boldsymbol{f}_{ext}$*

Before needle cuts into tissue as shown in Fig. 2(a), the external force applied by needle on tissue is simply modeled by Hooke's law:

$$\boldsymbol{f}_{ext} = k(\boldsymbol{x}_n - \boldsymbol{x}_{e0}) \tag{8}$$

where k is the stiffness, and $\boldsymbol{x}_n$ is the needle tip position, and $\boldsymbol{x}_e$ is the nearest nodal position, and $\boldsymbol{x}_{e0}$ is its initial position. After needle cutting into tissue as shown in Fig. 2(b), the external force is calculated by:

$$\boldsymbol{f}_{ext} = k\sum_{i=1}^{m}(\boldsymbol{x}_n^i - \boldsymbol{x}_{e0}^i) \tag{9}$$

where m is the number of needle segments, $\boldsymbol{x}^i_n$ is the position of ith needle segment, $\boldsymbol{x}^i_{e0}$ is the initial position of node which is closest to the ith needle segment, and $\boldsymbol{x}^i_e$ is its current position.

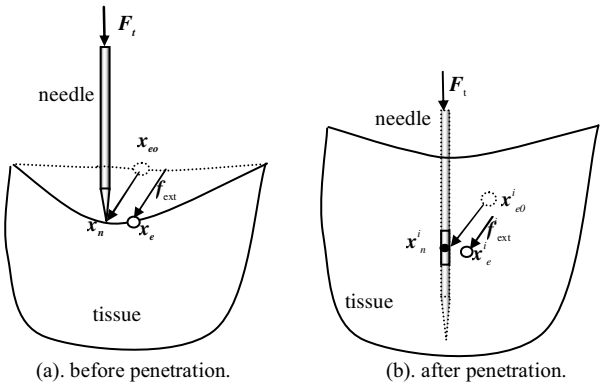

(a). before penetration. (b). after penetration.

Fig.2. Schematic of external force calculation.

III. FLEXIBLE NEEDLE MODELING

In this section, the models of needle buckling and deflection are proposed. It is noticed that only needle deformation outside tissue is considered, and the deformation inside tissue will be reported in our future work.

A. *Buckling*

A long, slender, ideal column under the action of an axial load will fail by buckling (see Fig. 3). Buckling is a failure mode characterized by a sudden failure of a structural member subjected to high compressive stresses, where the actual compressive stresses at failure are smaller than the ultimate compressive stresses that the material is capable of withstanding. The buckling effect is so large that the effect of the direct load may be neglected. In clinical practice, buckling of a flexible needle may cause difficulties in inserting the needle to desired location.

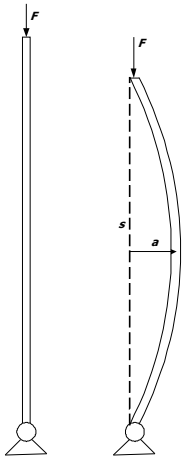

Fig. 3. Schematic of needle buckling.

In 1757, Euler derived a formula that gives the maximum axial load that a long, slender, ideal column can carry without buckling. An ideal column is one that is perfectly straight, homogeneous, and free from initial stress. The maximum load, sometimes called the critical load, causes the column to be in a

state of unstable equilibrium; that is, any increase in the load, or the introduction of the slightest lateral force, will cause the column to fail by buckling. The Euler formula for columns is:

$$P_e = \frac{\pi^2 EI}{l^2} \tag{10}$$

where P_e is the maximum or critical force (vertical load on column), E is the modulus of elasticity, I is the area moment of inertia, and l is the unsupported length of column.

B. Large deflection

Consider an elastic column of length l and bending rigidity EI in 2D as shown in Fig. 3. When the axial compressive forces F are applied at both ends of the column, the deflection w(x) takes place in the following form:

$$w(x) = a\sin(\frac{\pi x}{s}) = \frac{s}{\pi}\tan(\alpha)\sin(\frac{\pi x}{s}) \tag{11}$$

where a is the maximum deflection, x varies from 0 to s, s is the span of the beam and α is the slope angle at ends. α can be numerically calculated according to [2]:

$$\int_0^{\pi/2} \frac{dw}{\sqrt{1-\sin^2\frac{\alpha}{2}\sin^2 w}} = \frac{\pi}{2}\sqrt{\frac{F}{F_e}} \tag{12}$$

where F_e is the Euler buckling load as in (10), and F is the loading force applied on needle which will be explained in next section. Using (10), we can rewrite above equation as:

$$\int_0^{\pi/2} \frac{dw}{\sqrt{1-\sin^2\frac{\alpha}{2}\sin^2 w}} = \frac{l}{2}\sqrt{\frac{F}{EI}} \tag{13}$$

IV. Force Modeling

An energy-based method, similar to the way proposed in [4], is used to model force which will be sent to a user through our haptic interface during needle insertion process. Accounting for all energy terms entering an energy balance equation, the law of energy conservation applied between two consecutive states at times t and $t+\Delta t$ yields:

$$\Delta W_e = \Delta U + \Delta W_c \tag{14}$$

where ΔU is the change of elastic potential energy which can be calculated with FEM, ΔW_e is the external work applied by the needle, and ΔW_c is the irreversible work of cutting. In the case of elastic fracture, the work required to propagate a crack of unit of area inside a body is specific to a material and is called its fracture toughness J_c. In the quasi-static case (kinetic energy is neglected), W_c is entirely consumed by the crack formation [3]. Given a crack s of area $a(s)$, this work is given by:

$$W_c = J_c a(s) \tag{15}$$

For needle insertion as shown in Fig. 4, ΔW_c can be calculated as:

$$\Delta W_c = 2\pi J_c r \Delta l \tag{16}$$

where r is the needle radius and Δl is the insertion depth increase. ΔW_e is a function of the tool displacement, Δx, and of the force F_t it applies:

$$\Delta W_e = F_t \Delta x \cos\theta \tag{17}$$

where θ is the angle between F_t and insertion direction. From above equations, we can obtain the reaction force F_h for haptic rendering:

$$F_h = -F_t = -(\frac{\Delta U}{\Delta x\cos\theta} + \frac{2\pi J_c r\Delta l}{\Delta x\cos\theta}), \quad (0 < \theta < \frac{\pi}{2}) \tag{18}$$

The entire process of needle insertion can be reduced to two stages: deformation and penetration. If the exerted force F_t on the tissue is smaller than the tissue rupture force F_r, the tissue will only deform and won't be ruptured as depicted in Fig. 4(a). Otherwise, deformation and penetration will be observed (Fig. 4(b)). In deformation stage, the work done by a needle is transferred into elastic energy U, stored in deformed tissue. The tissue recovers to initial states with releasing of the elastic energy if the exerted force is removed. While in penetration stage, the work W_e done by a needle equals to the summation of the elastic energy U and irreversible work W_c spent on tissue piercing.

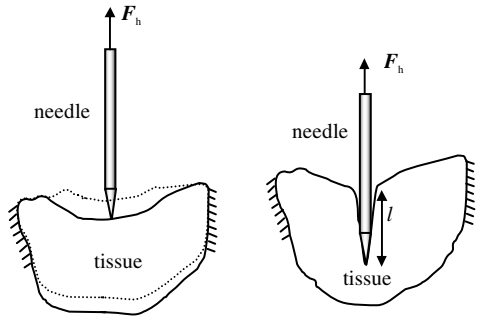

(a). before penetration. (b). after penetration.

Fig. 4. Schematic of haptic rendering.

V. An Experimental Case Study

Based on the above described modeling methods of tissue deformation, flexible needle buckling and deflection, and haptic rendering, a flexible needle simulator is developed as shown in Fig. 5. The system is configured as follows: Dell® precision PWS670; a dual-processor Xeon (TM) 2.8 GHz with 1GB RAM; NVIDIA Quadro graphic card; Microsoft Windows XP operation system; a Phantom® Premium 1.5/6-DOF device. OpenHaptics (SensAble®) API for haptic rendering. OpenGL® is used for graphic rendering.

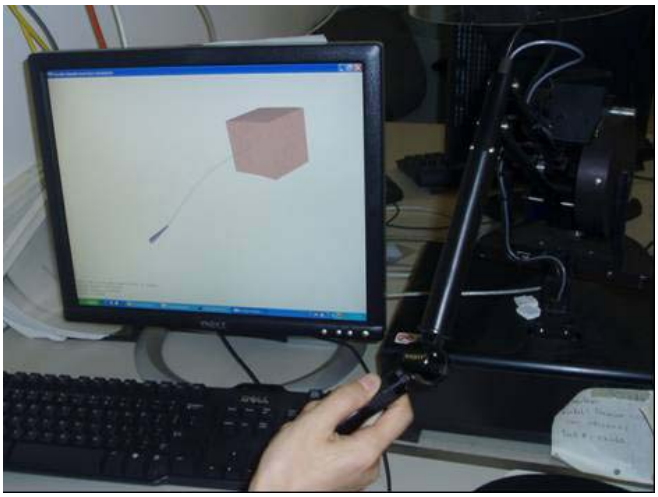

Fig.5. System setup of the flexible needle insertion simulator based on haptic interface.

In this simulator, a user can pick up a virtual needle by means of a haptic interface, Phantom Premium® 1.5. The needle parameters, e.g. radius and length can be arbitrarily selected. When the needle tip touches the tissue, the tissue will be deformed and the user can feel feedback force through the haptic interface. If the user further pushes the needle, it may buckle and deflect as shown in Fig. 6(b). If the external force applied on the tissue is larger than its rupture force, then the needle will pierce into the tissue. And the needle deflection will disappear (Fig. 6(c)). The feedback force will increase as the user further inserts the needle into tissue. The buckling force is dynamically updated using (10) as the length of needle outside the tissue decreases. If the driving force is larger than the buckling force, the second buckling will be observed as shown in Fig. 6(d). If the user selects a needle with short enough length or big enough radius, the needle buckling and deflection won't be observed during the insertion process. The parameters of needle and tissue are listed in Table 1.

TABLE I
Parameters of needle and tissue in the simulation.

Needle	length	radius	Young's modulus
	200 mm	0.3 mm	200 Gpa
Tissue	Young's modulus	Poisson ratio	mass density
	25 kpa	0.48	1.0 g/ml

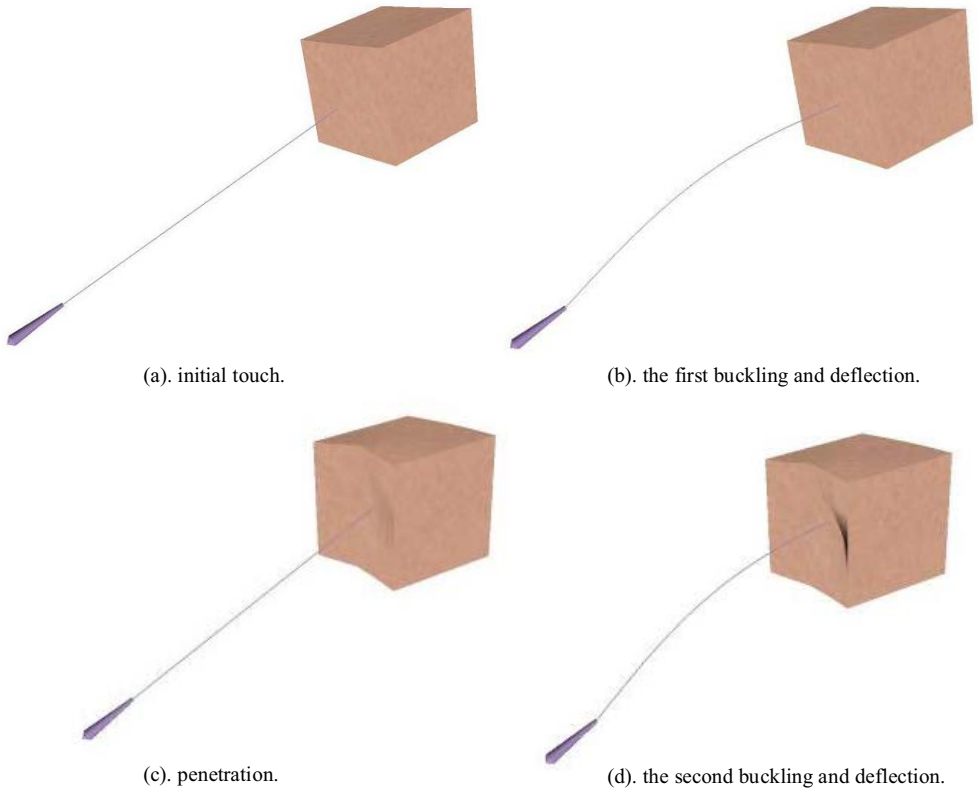

(a). initial touch.

(b). the first buckling and deflection.

(c). penetration.

(d). the second buckling and deflection.

Fig. 6. Screen shots of the process of needle insertion simulation.

The influence of needle parameters to insertion process is illustrated as shown in Fig. 7. In the first experiment, the needle radii are set to 0.3 mm. As seen from Fig. 7(a), when the needle length equals to 150 mm, the driving force increase almost linearly while the needle is inserted into the tissue before it penetrates the tissue. When the driving force is larger than the rupture force (e.g. 1.0 N), the needle pierces into the tissue and the force decreases rapidly. Then, the force

increases as the needle is further inserted into the tissue. When the needle length is set to 200 mm, force fluctuates before tissue is penetrated, which is attributed to needle buckling. As the length is set to 300 mm, the needle buckling occurs with smaller driving force. In the second experiment, the needle length is set to 200 mm with varying radius. Similar trend as seen from Fig. 7(b) is observed with the decrease of the needle radii.

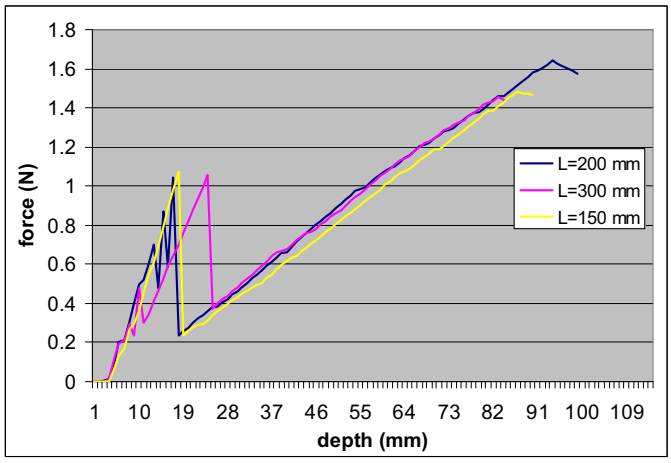

(a). the reaction force varies with needle length (r=0.3 mm).

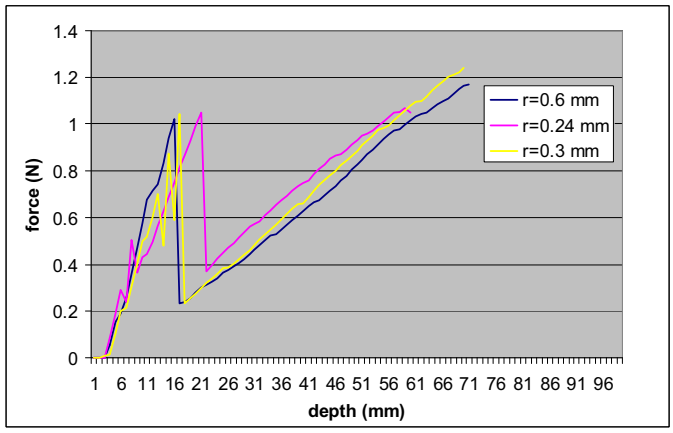

(b). the reaction force varies with needle radius (L=200 mm).

Fig. 7. Plots of reaction forces recorded from haptic interface during needle insertion process.

VI. Conclusions and Future Work

In this paper, a flexible needle insertion simulation system is proposed and implemented. It is based on the modeling methods of tissue deformation, flexible needle buckling and deflection, haptic rendering. A co-rotational FEM is used to model the tissue deformation. The external force applied to tissue by a needle is simply modeled using Hooke's law. The needle buckling and deflection is modeled according to beam-columns theory. A fracture mechanics approach is used to model the feedback force for haptic rendering. Through this system, a user can better understand the flexible needle insertion process which is different from traditional ones.

Many aspects need to be further considered and improved since the system is still in an early stage. During the insertion process, the mesh topology modification is not taken into account since the needle radius is always smaller than 1mm. The technique of dynamic mesh subdivision is commonly used in the simulation of needle insertion, e.g. [5]. However, it might increase the computation complexity and induce system instability. Therefore, for the time being, the mesh is subdivided in advance along the insertion path before the tissue model file is loaded into the system as shown in Fig. 8. Currently, the tissue model in this paper is homogeneous. In future, function gradient materials (FGM) will be modeled to investigate the flexible needle deformation in heterogeneous and multi-material tissues. The validation of the tissue deformation model will also be taken into account in future.

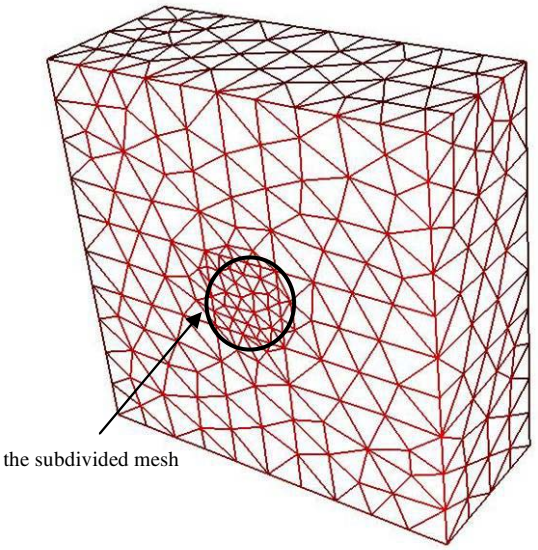

Fig. 8. Mesh subdivision at the insertion area.

References

[1] M. Müller, J. Dorsey, L. McMillan, R. Jagnow, and B. Cutler, "Stable real-time deformations," Proceedings of ACM SIGGRAPH Symposium on Computer Animation, pp. 49-54, 2002.

[2] Chen, W. F. and Atsuta, T., Theory of Beam-Columns, vol. 2, McGraw-Hill, 1977

[3] Atkins A. G., Mai Y-W., "Elastic and plastic fracture: metals, polymers, ceramics, composites, biological materials," Chichester: Ellis Halsted Press, 1985.

[4] M. Mahvash and V. Hayward, "Haptic Rendering of Cutting, A Fracture Mechanics Approach," Haptics-e, The Electronic J. Haptics Research, vol. 2, no. 3, 2001.

[5] Simon P. DiMaio, "Interactive Simulation of Needle Insertion Models," IEEE transactions on biomedical engineering, vol. 52, no. 7, p. 1167-1179, 2005.

[6] E. Gobbetti, M. Tuveri, G. Zanetti, and A. Zorcolo, "Catheter insertion simulation with co-registered direct volume rendering and haptic feedback," in Proc. Medicine Meets Virtual Reality 2000, Jan. 2000, pp. 96-98.

[7] T. Dang, T. M. Annaswamy, and M. A. Srinivasan, "Development and evaluation of an epidural injection simulator with force feedback for medical training," in Proc. Medicine Meets Virtual Reality, 2001, pp. 97-102.

[8] C. Simone and A. Okamura, "Modeling of needle insertion for robot assisted percutaneous therapy," in Proc. IEEE Int. Conf. Robotics and Automation, May 2002, pp. 2085-2091.